Process Safety and Environmental Protection 175 (2023) 665–676

Contents lists available at ScienceDirect

Process Safety and Environmental Protection

journal homepage: www.journals.elsevier.com/process-safety-and-environmental-protection

Polymer functionalized Hazel Sterculia hydrogel beads for adsorption of anionic azo dye RR120 from industrial streams

Anjani R.K. Gollakota [a,b,*], Munagapati Venkata Subbaiah [c], Chi-Min Shu [a,**], Prakash K. Sarangi [d], Jet-Chau Wen [a,c]

[a] Department of Safety, Health and Environmental Engineering, National Yunlin University of Science and Technology, Douliu City 64002, Yunlin County, Taiwan, ROC
[b] Department of Chemical and Materials Engineering, National Yunlin University of Science and Technology, Douliu City 64002, Yunlin County, Taiwan, ROC
[c] Research Centre for Soil & Water Resources and Natural Disaster Prevention (SWAN), National Yunlin University of Science and Technology, Douliu city 64002, Yunlin County, Taiwan, ROC
[d] College of Agriculture, Central Agricultural University, Imphal, Manipur, India

ARTICLE INFO

Keywords:
Hazel sterculia
Chitosan
Sodium alginate
Reactive red 120
Adsorption

ABSTRACT

Biomass (Hazel Sterculia seed-HS) was functionalized with chitosan and sodium alginate polymers to synthesize novel sorbent materials for the extraction of anionic reactive red 120 dye molecules from aqueous streams. Sodium alginate functionalized biomass (HSSA) and chitosan functionalized biomass (HSCS) were generated using a 1:1 ratio throughout the functionalization process. Characterization techniques (XRD, FTIR, SEM, and BET) showed that the functionalization process effectively modified the morphological properties of the raw biomass, including an increase in surface area from 1.03 m^2/g to 7.81 m^2/g (HSCS) and an increase to 5.58 m^2/g (HSSA). Similarly, batch adsorption studies were conducted with varying starting dye concentrations (10–1000 mg/L), adsorbent dosages (0.05–0.15 g), contact times (0–360 min), agitation speeds (100–500 rpm), and pH (1−10). The Langmuir and Freundlich isotherm models were used to learn more about the adsorption process. Maximum adsorption capacities of 79.35 mg/g (HSCS) and 60.27 mg/g (HSSA) were observed for Langmuir monolayer adsorption, respectively. In addition, kinetic modeling studies showed that pseudo-second order kinetics, with a regression coefficient of $R^2 > 0.99$, was a good fit for RR120 adsorption onto HSCS, HSSA. The thermodynamic properties showed that the adsorption of RR120 onto the selected adsorbents was an endothermic, spontaneous process. Finally, regeneration studies verified that HSCS and HSSA sorbents could be recycled for three, and two cycles respectively.

1. Introduction

Global development has caused tremendous water pollution especially the changing fashion trends among societies inspired textile manufacturers to use different classes of dyes (Foroutan et al., 2021), causing serious groundwater table pollution. Apart from textile industries, pharmaceuticals, food, leather, and paint industries have parted their ways in using dyes and disturbing the blue planet (Pashaei-Fakhri et al., 2021). Already humans, and aquatic lives are seriously endangered due to the consumption of this toxic dye contaminated water, and at places the water is completely unusable even for potable consumption. Among which, toxic azo dyes contribute 15–50% of total discharges (80%) from textile effluent streams (Al-Tohamy et al., 2022). To achieve consistent hues and a low environmental impact, synthetic dyes, such as reactive dyes, are widely utilized for the cotton dying process. The presence of aromatic diazo groups in the structure of azo dyes like RR120 makes them inherently stable and resistant to natural degradation, which poses a risk to the water supply and the food chain that depends on it (Jawad et al., 2020b, 2020c, 2020a; Jawad and Abdulhameed, 2020a, 2020b). The repercussion includes the toxic, mutagenic, and carcinogenic effects have already been reported for metabolities of reactive triazine dyes (e.g., aromatic amines) in laboratory animals exposed to them (Ahmadi et al., 2022; Foroutan et al., 2020; Mousavi et al., 2023). Further, these

* Corresponding author at: Department of Safety, Health and Environmental Engineering, National Yunlin University of Science and Technology, Douliu City 64002, Yunlin County, Taiwan, ROC.
** Corresponding author.
E-mail addresses: garkiran@yuntech.edu.tw (A.R.K. Gollakota), shucm@yuntech.edu.tw (C.-M. Shu).

https://doi.org/10.1016/j.psep.2023.05.083
Received 24 February 2023; Received in revised form 8 May 2023; Accepted 27 May 2023
Available online 29 May 2023

modern-day dyes replacing the traditional ones were highly resilient to chemical, photochemical, and biological degradation forcing an additional separation process. Hence, these synthetic dyes must be extracted from the effluent streams prior to discharging is much of interest. Ion exchange, membrane separation, photocatalytic degradation, coagulation-flocculation, chemical oxidation, and adsorption techniques are being developed to remove synthetic dyes from aqueous streams. Because its simplicity, affordability, and effectiveness, adsorption is considered the best option. But the greater challenge lies with the choice of raw material, and the synthesis of eco-friendly adsorbent.

Nevertheless, the development of adsorbent is receiving a lot of focus, and biopolymer materials are an excellent choice for this purpose. The biopolymer's potency as an adsorbent stems from the abundance of active adsorption sites, such as (–OH) and (–NH_2) groups (Sutirman et al., 2018). Chitosan (CS), and sodium alginate (SA) are such polymers composed of 2-acetamido-2-deoxy-D-glucopyranose and 2-amino-2--deoxy-D-glucopyranose monomers and the later is composed of homopolymeric blocks of (1−4)-linked -D-mannoronate and C-5 epimer -L-guluronate residues that are covalently bonded together (Gao et al., 2020). Furthermore, sodium alginate's carboxyl and hydroxyl functional groups electrostatically bind and chelate with ions, causing the substance to gel (Mohammed et al., 2022).

On the spin side, biomass based adsorbents invariably outperform their chemical counterparts due to their superior environmental friendliness, lower cost, higher surface properties, rich morphological functional moieties, and least chemical modification treatments (Sargin et al., 2016). In addition, improper processing of these biomass materials also results in ecological imbalances. Also, there was a very limited amount of literature available on the selected biomass waste (Hazel sterculia shell-HS), and its applicability as a sorbent material.

Thus the objective of the study is to combine the novel features of the polymer materials (CS, SA) to the rarely explored biomass HS to form the polymer cross-functionalized biomass adsorbent (HSCS, HSSA) and applied to treat the anionic dye RR120 from the contaminated aqueous streams. Further, to the best of the authors knowledge after rigorous literature there are no studies available for the current choice of cross functionalization. Furthermore, the efficacy of the newly synthesized sorbent materials were tested rigorously to optimize the key parameters of adsorption studies such as solution pH, point of zero charge (pH_{pzc}), influence of adsorbent dosage, initial dye (RR 120) concentration, and contact time. Besides, the isotherms (Langmuir, and Freundlich), kinetic studies (pseudo-first order, pseudo-second order), and thermodynamic functions namely Gibb's free energy (ΔG°), enthalpy (ΔH°), and entropy (ΔS°) were determined. Lastly, the adsorption mechanism of RR 120 dye onto HSCS, and HSSA adsorbents was proposed and discussed in detail.

2. Materials and methods

The purity of the reagents NaOH and HCl utilized in the current research was greater than 99%. Chitosan (200–400 MPa.s), sodium alginate (5–40 MPa.s), $CaCl_2$ (anhydrous powder ≥ 97%), RR120 dye (≥ 50% dye composition), acetic acid (≥ 99% purity), HNO_3, KOH, were obtained from Sigma-Aldrich, Taiwan. Further, biomass feedstock HS was prepared in the laboratory. Hazel Sterculia (HS) shells were collected from the YunTech campus and washed in running water to eliminate any remaining debris. Further, the shells were dried under sunlight for three days followed by the furnace drying at 50 °C for 24 h to eliminate the traces of moisture. Once the shells are completely dried, they were crushed in fine powder. Using deionized (DI) water and a calibrated Perkin Elmer UV-Vis spectrophotometer, we analyzed the adsorption of RR120 onto HSCS and HSSA. All the batch adsorption studies were performed thrice and the average values were reported.

2.1. Synthesis of adsorbents

2.1.1. Chitosan-Hazel Sterculia – HSCS

In 50 mL of 5% (m/v) acetic acid, 3 g of chitosan (low molecular weight, 75–85% deacetylated, Sigma-Aldrich) was dissolved. The gel was stirred for twenty-four hours to achieve total dissolution (Rorrer et al., 1993). Further 1:1 ratio of biomass was mixed to the prepared gel and allowed to thoroughly mix for 4 h on magnetic stirrer. Once the complete dissolution of HS:Chitosan happened, the mixture was dripped using micropipette of 1 μL into a NaOH 0.5 mol L^{-1} solution drop wise.

2.1.2. Alginate-Hazel Sterculia - HSSA

To make alginate gel beads, solutions of sodium alginate and calcium chloride (reagent grade, Fischer-Scientific) had to be made. On a hot plate at 60 °C with magnetic stirring, 150 mL of deionized water was used to dissolve 4.5 g of sodium alginate. To get to 200 mL of alginate solution, more deionized water was added throughout the solution dissolution process. $CaCl_2$ solution was prepared by dissolving 33.3 g of $CaCl_2$ in 1.5 L of deionized water with the aid of a stirring magnet. The mixture was allowed to completely dissolute for 12 h in a magnetic stirrer. Further, 1:1 ratio of HS to alginate was added slowly and allowed to dissolute completely after stirring for 6 h. The alginate-HS solution was then dropped into $CaCl_2$ solution using a peristaltic pump to produce alginate beads (Kahya and Erim, 2019). A stirring magnet continuously agitated the $CaCl_2$ throughout the process to prevent the accumulation of immature alginate beads. After preparing all of the alginate beads, they were thoroughly rinsed with distilled water. Finally, the alginate beads were suspended in a glass bottle and chilled to 4 °C in the refrigerator.

2.2. Preparation of the dye solution

Sigma-Aldrich Taiwan supplied the reactive red 120 (RR120) model textile reactive dye. RR120 dye was dissolved in 1000 mL of double-distilled water to prepare a stock solution with a concentration of 1000 mg/L. Sequentially diluting the stock solution with double distill water yielded dye solutions with concentrations ranging from 10 to 100 mg/L for use in treatment testing.

2.3. Adsorption studies

Adsorption experiments of RR120 utilizing HSCS and HSSA were conducted at 25 °C. 30 mL of dye solutions at varying concentrations and the optimal pH were used in each of a series of 100 mL volumetric flasks for each adsorption experiment. Dye solutions were pH-balanced with 0.1 N NaOH or 0.1 N HCl before experiments were performed. In each flask, 0.1 g (HSCS), 0.08 g (HSSA) of adsorbent with a predetermined particle size and dosage was introduced and agitated frequently at 100 rpm (HSSA), 300 rpm (HSCS) until equilibrium was attained (approximately 12 h). The solution was then filtered under vacuum, and the intake of RR120 was measured spectrophotometrically by measuring absorbance at $\lambda_{max} = 515$ nm. The mass balance of the dye molecule concentration, Eq. (1), was used to calculate the amount of RR120 dye molecules adsorbed onto the surface of the HSCS, HSSA, and the percentage of desorption was calculated using Eq. (2).

$$q_e = \frac{(C_i - C_e)V}{m} \tag{1}$$

$$\text{Desorption}(\%) = \frac{desorbed}{adsorbed} \times 100 \tag{2}$$

2.4. Characterization of adsorbent

To identify any existing phases and crystallinity, X-ray diffraction (XRD) patterns were produced using an x-ray diffractometer (Philips

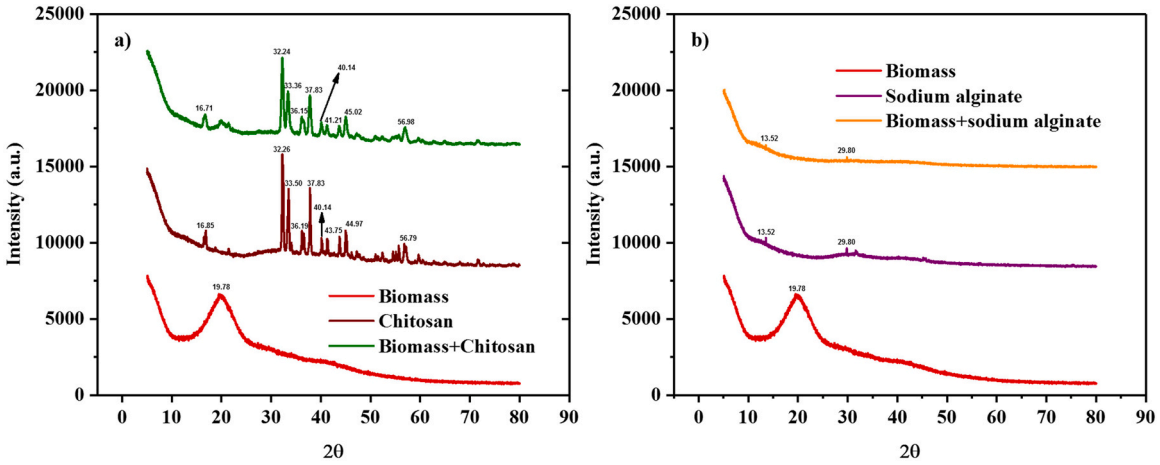

Fig. 1. XRD spectra of biomass in the scan range of 5–80° a) chitosan functionalized biomass (HSCS) b) sodium alginate functionalized biomass (HSSA).

X′Pert diffractometer) utilizing K radiation of (Cu-Kα) in a Bragg-Bretano configuration between 5 ° and 80 °, with a duration per step of 0.02 S. HSCS, HSSA, and Hazel Sterculia (HS) surface morphology was captured utilizing a field emission scanning electron microscope (FESEM, JEOL, JSM-7610 F Plus). Using a surface area analyzer, nitrogen adsorption isotherms at 77 K were used to determine the surface characteristics of the HS, HSSA, and HSCS samples (Micrometrics, ASAP 2060). The functional group of the synthesized materials were investigated between 4000 and 400 cm^{-1} using PerkinElmer Spectrum One Fourier transform infrared spectrometer (FT-IR). PerkinElmer Lambda 850 double beam spectrophotometer absorption spectra in the UV-Visible region (400–800 nm) were collected at room temperature, adjusted against an appropriate baseline, and zeroed off at 515 nm.

3. Results and discussion

3.1. XRD analysis

The crystal structure of the raw biomass (HS), chitosan (CS), sodium alginate (SA), after functionalizing the chitosan and sodium alginate onto the biomass were analyzed using the powder X-ray diffraction (Fig. 1). The adsorption patterns of the adsorbents show typical spectrum having main and secondary peaks upon scanning at the 2θ range of 5°–80°. From the, figure, the surface morphology of the biomass is mostly amorphous in nature with a major identification of peak at 2θ= 19.78°. A sharp peak between 18° and 22° owing the presence of crystalline cellulose in biomass (Awoyale and Lokhat, 2021). Further, the XRD characteristic peaks of commercial chitosan samples were found at 2θ = 37.82°, 44.06° (Kaya et al., 2014); while for sodium

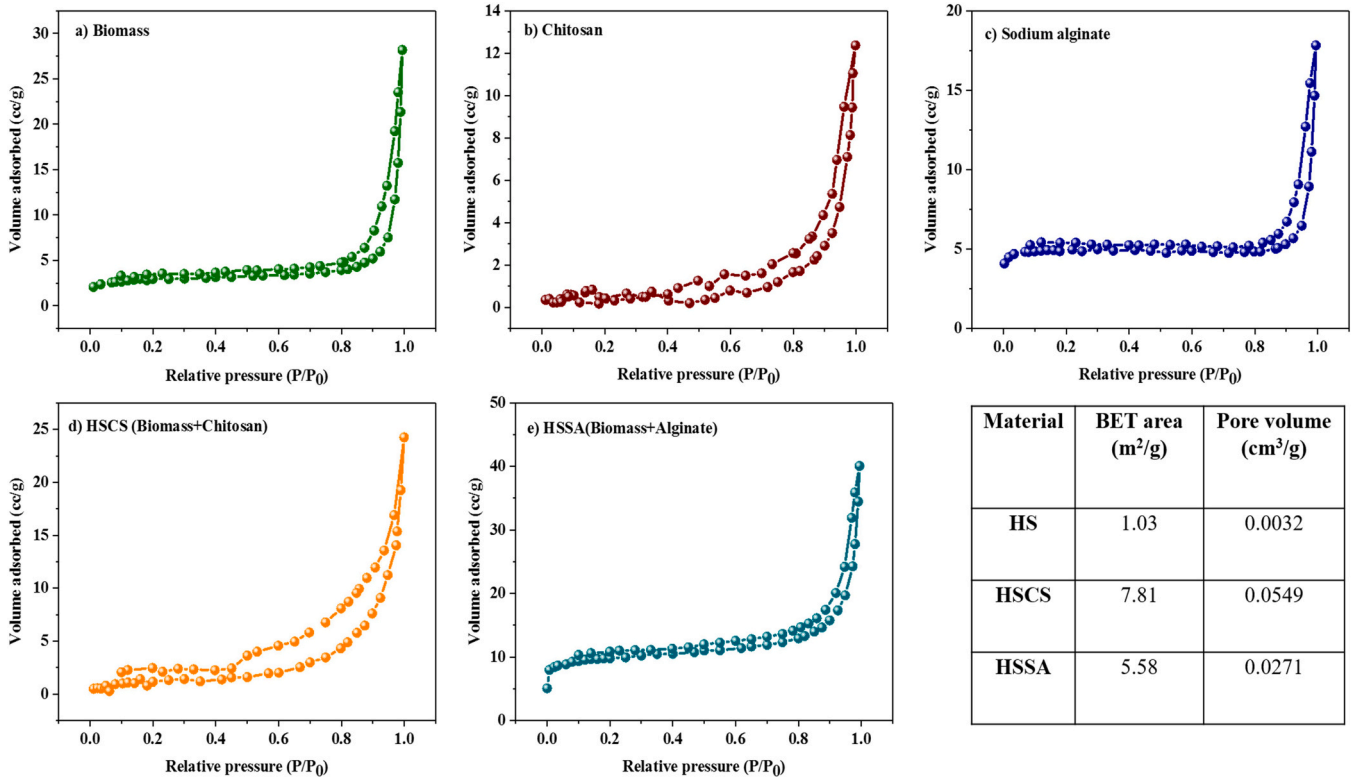

Material	BET area (m^2/g)	Pore volume (cm^3/g)
HS	1.03	0.0032
HSCS	7.81	0.0549
HSSA	5.58	0.0271

Fig. 2. N_2 adsorption-desorption isotherms (a) raw HS; (b) Chitosan (c) Sodium alginate (d) HSCS (e) HSSA.

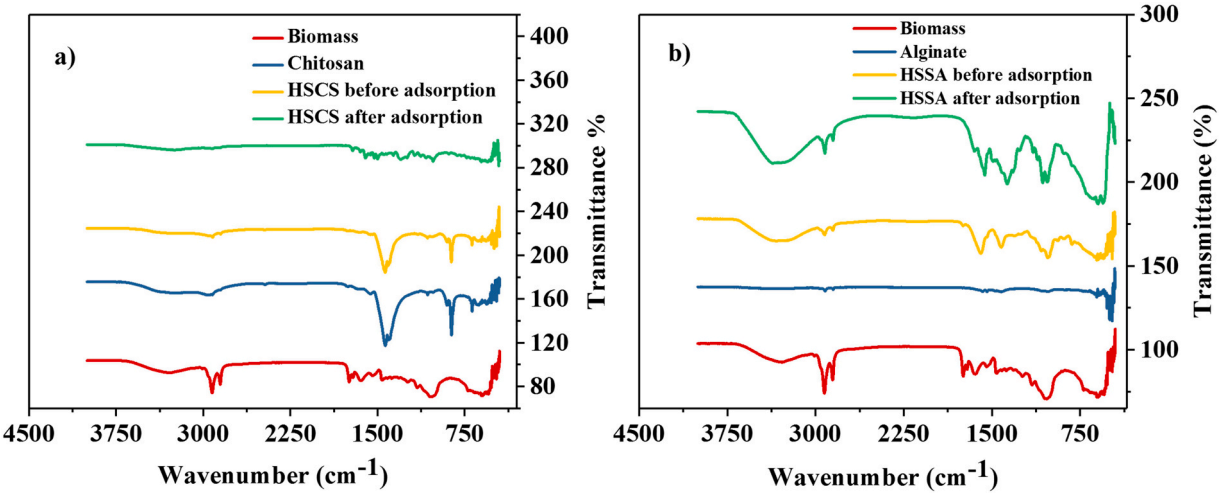

Fig. 3. FT-IR spectrum (scan range of 400 – 4000 cm^{-1}) before and after functionalization of (a) biomass, chitosan, HSCS before adsorption, HSCS after adsorption b) biomass, sodium alginate, HSSA before adsorption, HSSA after adsorption.

alginate, the peaks were identified at 2θ = 13.5°, and 29.8° (Abid et al., 2021). Upon functionalizing the biomass with polymers (chitosan and alginate) the XRD diffractogram clearly represents no prominent deviation of the peaks except the intensity. This intensity reduction might be attributed to the changing the crystallinity to the amorphous phase otherwise indicating the embedment of the polymer on to the surface of the biomass adsorbent. Moreover, chitosan molecules readily form crystalline areas, which may be attributed to the abundance of –OH and $–NH_2$ groups in the structure of chitosan, which can build stronger intermolecular and intramolecular hydrogen bonds (Kaya et al., 2014). Therefore, it can be concluded that the intensity was the primary criterion for detecting functionalization, and that functionalization reduced crystallinity in both chitosan and alginate.

3.2. Pore characteristics

Nitrogen adsorption/desorption isotherms of pre and post functionalization of biomass with chitosan and sodium alginate along with individual compounds were presented in Fig. 2. The adsorption isotherms for these samples are classified as Type II by the International Union of Pure and Applied Chemistry (IUPAC). These isotherms are typically observed in adsorbents with a wide range of pore sizes, i.e., microporous. Type II isotherms have an inflection point that occurs after the first adsorption monolayer is formed and continues to ascend with increasing relative pressure until an infinite saturation number of adsorption layers has been formed (Lowell and Shields, 1991). Besides, the adsorbate molecules have strong mutual interactions, which leads to a multilayer adsorption. Further type II isotherms correspond to systems involving capillary condensation in porous solids tends to dominate at high relative pressure ($P/P_0 > 0.83$). In addition, hysteresis loops were shown to be associated with the adsorbent's texture; thus, this phenomenon is characterized by the H4 hysteresis definition (Anfar et al., 2020). The presence of micropores and mesopores in a material is indicative of complexity, as suggested by the H4 hysteresis. The hysteresis loop closure is characterized by a stepdown in the desorption branch, which is present in this hysteresis.

3.3. FTIR analysis

The FTIR transmittance spectra of pure biomass, chitosan, sodium alginate, biomass functionalized chitosan, sodium alginate prior and after adsorption of RR120 are shown in Fig. 3. The C–O stretching in cellulose, hemicellulose, and planar polysaccharides elicited strong peaks in the biomass spectrum at 1041 and 1239 cm^{-1} (Acquah et al., 2016). Other intense peaks at 1641 cm^{-1} (Bekiaris et al., 2020), 1403 cm^{-1} are associated with the C═O stretching vibration, whereas peaks at 2854 cm^{-1} (Nitsos et al., 2018), 2924 cm^{-1} (Liu et al., 2016) are related with the asymmetric stretching vibrations of the CH_2 groups. In the case of pure chitosan, the intense bands at 1418 cm^{-1} (Varma et al., 2021) and 1433 cm^{-1} (Adel et al., 2019) depict CH_2 bending mode vibrations, with the other representative bands at 863 (Varma et al., 2021), 1069 cm^{-1} (Huang andChu, 2013), 1561 cm^{-1} (El-Hefian et al., 2010), and 2919 cm^{-1} (Mishra et al., 2013) denote C–N stretching, C–O skeletal vibrations, NH bending vibration of amine groups, and C–H stretching respectively. For pure sodium alginate, only two peaks appear at 1035 cm^{-1} (Kuczajowska-Zadrożna et al., 2020a) and 1405 cm^{-1} (Kuczajowska-Zadrożna et al., 2020b). The former shows the presence of –COC groups, while the latter is ascribed to the existence of carboxyl groups by oscillations of COO^- groups. In addition, the adsorption peaks in the range of 3200–3600 cm^{-1} were mainly assignable to O-H stretching vibrations (Sabater i Serra et al., 2020).

Upon functionalizing biomass with chitosan and alginate, the FTIR spectra was saliently altered, with the disappearance of some peaks and the development of other peaks, indicating the exchange of functional groups. For chitosan-functionalized biomass, four additional spikes were identified at 865 cm^{-1} (Abdolrahimi et al., 2018), 1436 cm^{-1} (Gaabour, 2017), 2849 cm^{-1} (Heba and Ali, 2023), and 2919 cm^{-1} (Mishra et al., 2013), confirming the C–N stretching, C–O skeletal vibrations, NH bending, C–H stretching. Further, adsorption of the RR 120 dye onto the surface there observed a shift and the intensity of the peaks confirms the sorption phenomenon. In the case of biomass functionalized with sodium alginate, however, a significant difference was detected with the emergence of new peaks at 1033 and 1023 cm^{-1} corresponding to the C–O stretching vibrations of polysaccharide pyranose rings. The further peaks at 1419 cm^{-1} (Pereira et al., 2011), 1594 cm^{-1} (Sarwar et al., 2021), and 2924 cm^{-1} (Li et al., 2021) represent the stretching vibrations of COO groups, COO^- asymmetric stretching, and –CH stretching vibrations, respectively. Similarly after the adsorption the critical intensity of some of the peaks were reduced and while some others were increased alongside the minor shifts indicating the interaction of dye and sorbent. In summary of the FTIR spectra, the exchange of functional groups across the biomass, chitosan, and sodium alginate was established.

3.4. Scanning electron microscopy

The SEM images of the pure biomass, chitosan, alginate and biomass functionalized chitosan, sodium alginate composite derivatives prior

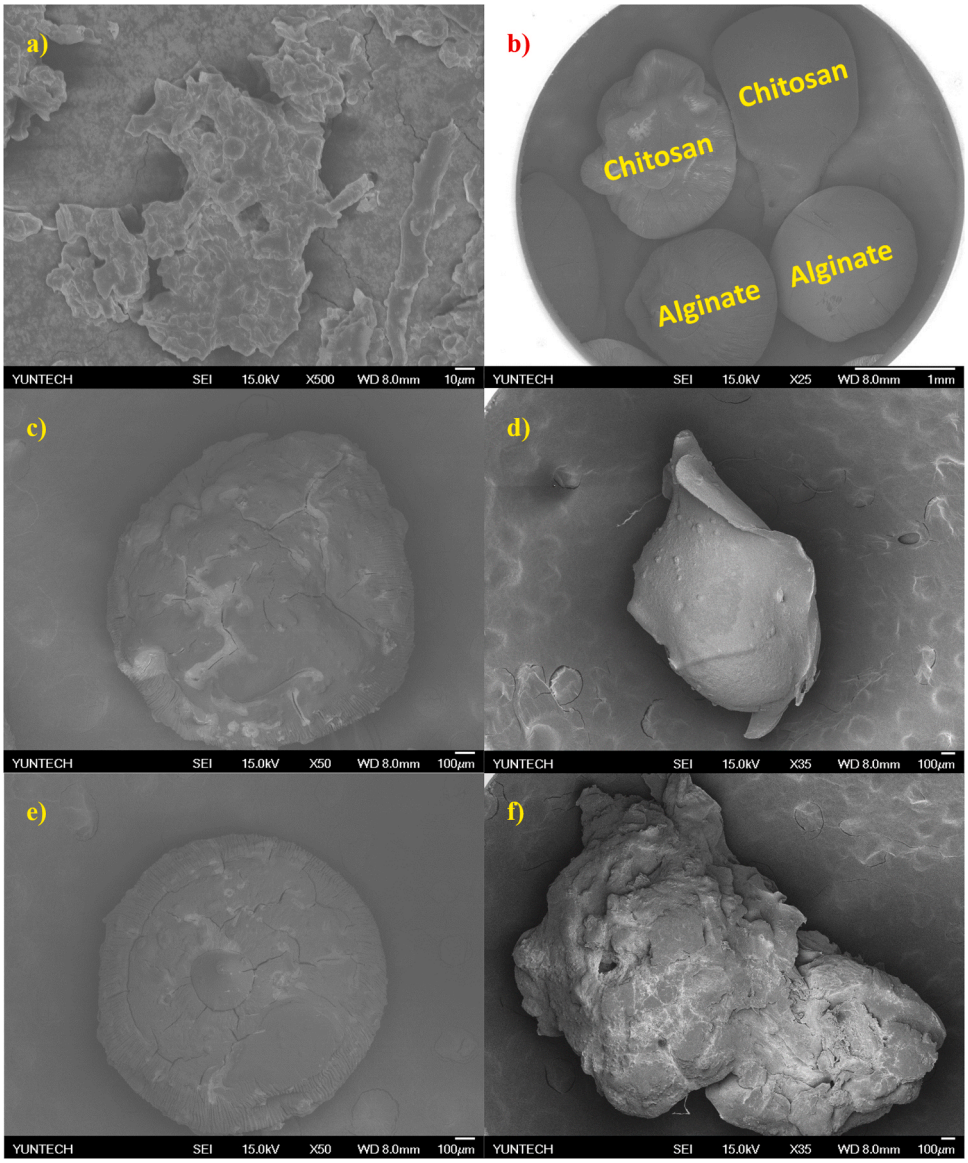

Fig. 4. SEM micrographs (magnification range of 25– 500 X) of (a-b) raw biomass (HS); and (c-d) HSCS prior and after adsorption; (e-f) HSSA prior and after adsorption.

and after adsorption of RR120 dye are shown in Fig. 4. The structural changes on the raw biomass had a smooth intact with a fibrillary morphology. Additionally, HS particles have no discernible shape and are widely dispersed, uneven, and heterogeneous (see Fig. 4a) (Gollakota et al., 2022a). Pure Chitosan have a membranous phase that was smooth and contained dome-shaped openings, micro fibrils, and crystallite (see Fig. 4b). It is possible that the loss of water during the drying process of chitosan is responsible for the crystal beads smooth texture and uneven surface (Bat-Amgalan et al., 2021). In case of the sodium alginate beads, the appearance resembles the golf ball with rough surface, and small dimples attributing the inter connected pore structure due to the hydration (see Fig. 4b) (Mansfield et al., 1999). Upon functionalizing the biomass with the chitosan, the morphological change was notable with relatively rough surface compared to pure chitosan (see Fig. 4c). In addition, the beads had wide pores that may have resulted from the incorporation of air during the production process (Kim, 2021). Moreover, after the adsorption of RR120 onto the surface there was an impressive change observed in the morphology of the sorbent material seems a smooth layer representing the total filling of adsorbent surface pores (see Fig. 4d). Similarly, the alginate functionalization on biomass resulted rough morphology with wide pore openings when compared to the pure alginate beads prior to the adsorption (see Fig. 4e). Whereas Fig. 4f represents the formation of layer and the change on the morphology clearly indicates the surface was occupied by the RR 120 dye and confirms the adsorption phenomenon. This indicates that the functionalization substantially altered the surface morphology of biomass that is lineated with the FTIR analysis. The newly formed morphology helps to expedite the interaction with the RR120 and its uptake on to the surface of the adsorbent molecules.

3.5. *Influence of pH*

pH is an influential parameter to check the efficiency of the biosorbents for the exclusion of dye from aqueous media, since it affected the solution chemistry as a well as the sorbent surface. Besides, the pH value of adsorption is a crucial parameter for determining the strength of the electrostatic charges existing in the solution or carried by the ionized dye particles present in the solution. At low pH values, it was discovered that the removal ratio for positive dyes drops and increases for negative dyes, as depicted in Fig. 5a. In the range of pH 1–3, the maximum

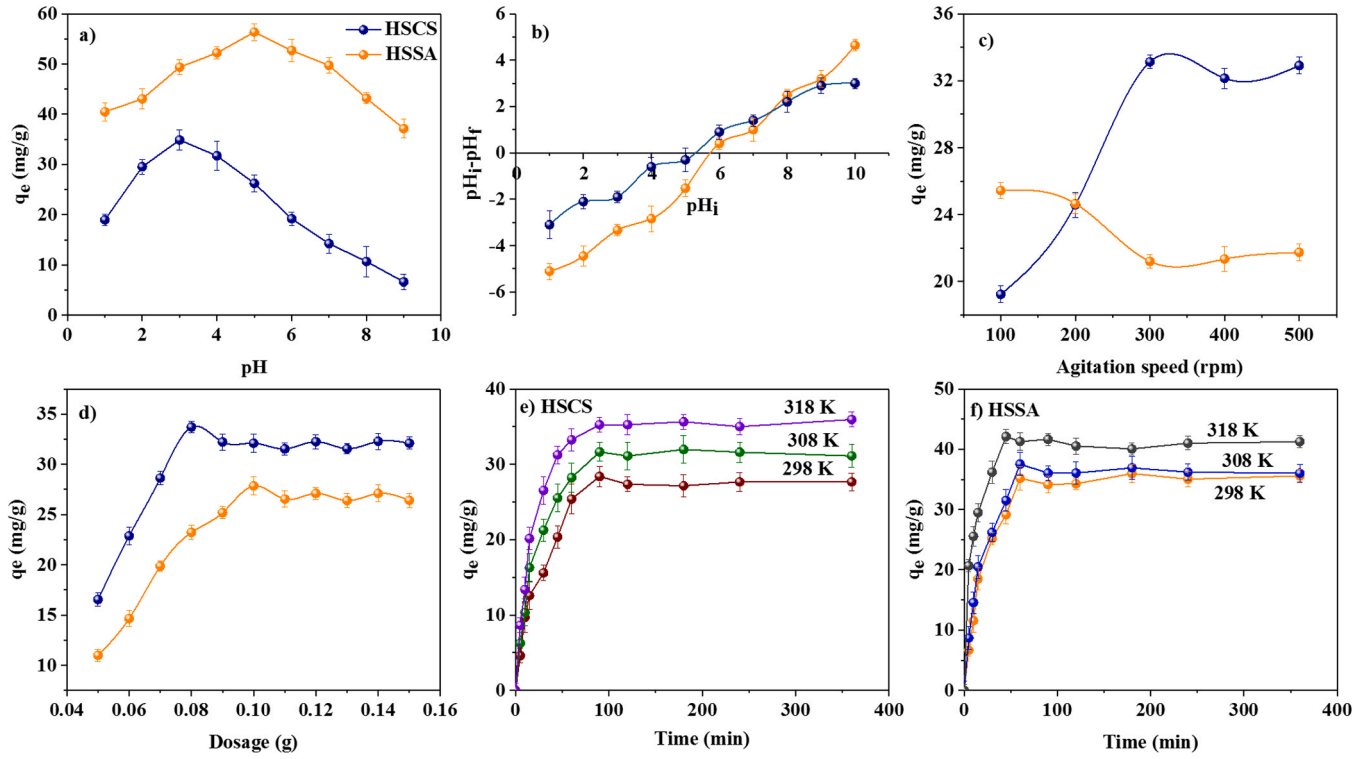

Fig. 5. Effect of various parameters on the adsorption of RR120 onto HSCS, HSSA (a) pH (2−10); (b) pHpzc; (c) dosage (0.05–0.15 g); d) agitation speed (100–400 rpm); (e–f) adsorption isotherm models.

adsorption capabilities of RR120 were obtained upon adsorption with HSCS. This may be because of the electrostatic interaction between the dye and chitosan molecules. The degree of deacetylation and neutralization of the amine groups also affects the pK_a of chitosan. Below pH 6.5, the majority of the amine groups were protonated, and this protonation is strongly considered to be responsible for the attraction of anionic sulphonic groups (Szygula et al., 2008). Sorption effectiveness dropped dramatically beyond pH 3, as the density of accessible sorption sites decreased.

Similar trends were reported for biomass cross-linked sodium alginate i.e., the dye sorption was reported maximum under acidic conditions (pH 5) and decreased in alkaline medium. Resin networks shrank under highly acidic conditions (pK_a 3.2), indicating that dyes cannot readily adsorb to them. This happened when the pH of the surrounding environment falls below 3. Fig. 5a demonstrates that the composite and dye molecules were more likely to form hydrogen bonds when the pH increased from 3 to 5. This was because the composite's carboxyl and sulfonic acid groups existed as –COOH and $–SO_3H$ at these pH levels (Zhu et al., 2017). In addition, the impact of pH and surface charge fluctuations on the adsorption process can be evaluated using point of zero change analysis (pH_{pzc}). The process was clearly stated (Gollakota et al., 2023) and have implemented the same for the present studies. Fig. 5b represents the point of zero charge analysis of the polymer (chitosan, sodium alginate) functionalized sorbent (biomass) materials. The infliction point of HSCS was reported to be 5.23; whereas it is 5.78 in case of HSSA which is greater than the actual pH for the adsorption of RR120. It is known that the solution pH less than the point of zero charge indicates that the net surface charge on the solid surface for the adsorbent becomes positive due to protonation of ions. These positive and negative charges favored the adsorption of anionic dye RR120 under acidic conditions indicating the electrostatic attraction, and other banding forces, such as hydrogen bonds and van der Walls forces too (Bensalah et al., 2017).

3.6. Influence of agitation speed

The effectiveness of the adsorption process is enhanced by the agitation speed by distributing the solute throughout the solution phase and creating an outer boundary layer. Further, the increase in the sorption with the increasing speed represents the better contact between the sorbent and sorbate at higher speeds. To a large extent, the rate of agitation governs the rate of mass transfer across the solid-liquid interface by affecting the density of the external flow separation and the distribution of solute particles in the solution (Patra et al., 2022). This was investigated by testing the effects of changing the agitation speed from 100 to 500 rpm on the adsorption of RR120 onto the surfaces of HSSA and HSCS at pH 5, and 3 respectively, at room temperature. Maintaining other conditions constant, the effect of changing the agitation speed on the adsorption process is seen in Fig. 5c. The highest percentage of RR120 dye removal from the solution was seen at 200 rpm speed which is 25 mg/g for HSSA and 35 mg/g for HSCS at 300 rpm. Adsorption is diminished at lower rpm values because mass transfer between the adsorbate and adsorbent is reduced as the rpm is increased. This is because the film boundary enclosing the particles is reduced (Geethakarthi and Phanikumar, 2011). The boundary layer becomes extremely thin and, at high agitation speeds, approaches the laminar sub-layer when the value of the external diffusion coefficient grows (Gollakota et al., 2021).

3.7. Effect of adsorbent dosage

High dye concentrations are predicted to yield superior adsorption results. The adsorption process was studied in the 0.05–0.15 g range while maintaining the other adsorption parameters at 300 mg/L dye concentration, pH 5 (HSSA), 200 rpm (HSSA), and pH 3 (HSCS), 300 rpm (HSCS) agitation speed. From Fig. 5d, it was found that the dye uptake tendency increased from 15 to 36 mg/g for HSCS from 0.05 to 0.08 g dosage. Similar trend was observed i.e., increasing dye adsorption capacity from 10 to 27 mg/g for HSSA in the range of 0.05–0.1 g of

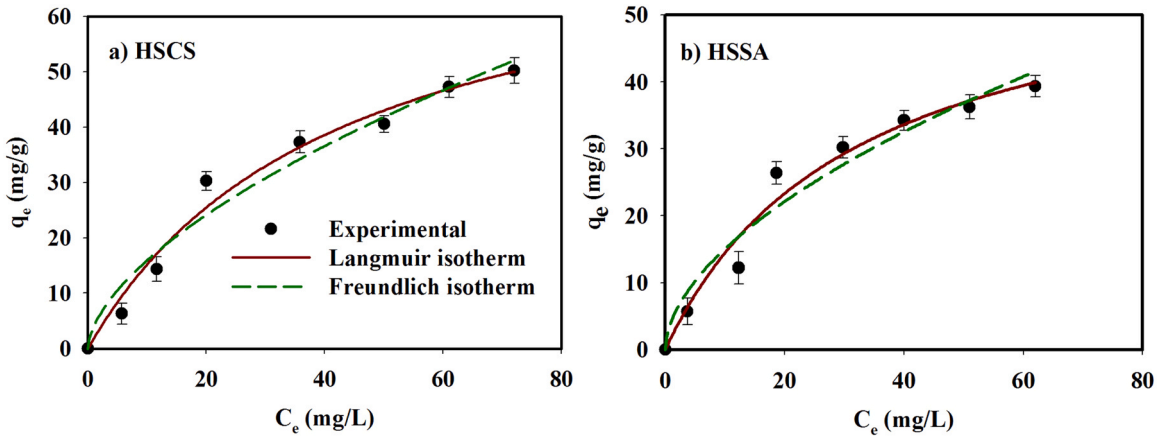

Fig. 6. Non-linear adsorption isotherm model studies with RR120 initial dye Concentration ranging between (10–100 mg/L) (a) HSCS; (b) HSSA.

dosage. The reason beyond the increasing adsorption rate with dose is primarily associated with the increasing number of available vacant adsorption sites on the surface of the adsorbent (Pourjavadi et al., 2015). Further increasing the dosage rates led to the declining trend of the dye adsorption which might be due to the fact that the substantial portion of the accessible adsorption sites remain exposed, favoring less per gram adsorption (Singh and Choden, 2014). In other words, when the amount of adsorbent in grams increases, the total surface area accessible for the adsorption of RR120 decreased due to site overlap or aggregation.

3.8. Effect of initial dye concentration

There is a theoretical limit to how different adsorbate species can be held by a given adsorbent. As a result of its high initial concentration, the dye is able to penetrate the solid phase, where it can then stay permanently despite the mass transfer obstacle between the aqueous and solid phases (Gollakota et al., 2021). Experiments were conducted with varying initial concentrations of RR120 while keeping all other parameters constant to assess the influence of starting dye concentration on adsorption efficiency. Adsorption capacity of RR120 was shown to increase with increasing concentration, suggesting that the initial dye concentration greatly affects the adsorption of RR120 onto HSCS, and HSSA. Since dye molecules must first traverse the liquid film from the bulk solution to the adsorbents external surface before entering the adsorbents pores, the amount of dye that was adsorbed onto the adsorbent is directly proportional to the concentration of the dye solution (Bazrafshan et al., 2013). Adsorption capacity is proportional to the amount of adsorbent present, hence for a given dose, the number of accessible sites does not change drastically. It makes sense that a higher proportion of active desorption sites would be available at a lower concentration for particles. Consequently, the adsorption capacity increases as the dye concentration rises. Hence, for the present adsorption studies the initial dye concentration of 30 mg/L was considered throughout the study.

3.9. Isotherm studies

The adsorption process of the HSCS, and HSSA adsorbents were modeled using an adsorption isotherm. The equilibrium amounts of dye in the solution and the dye adsorption onto the solid phase are also related by the isotherms. In addition, the experimental data was characterized using an isotherm analysis, which works best when the correlation coefficient (R^2) is close to 1. R^2 values close to one indicate agreement between the experimental data and the modeled isotherm. Both the Langmuir and the Freundlich isotherm models were applied to equilibrium adsorption data in order to determine the maximum adsorption capacity and the average free energy of adsorption. The non-linear forms of Langmuir (Langmuir, 1918) and Freundlich (Freundlich, 1907) equations are as follows:

Table 1
Equilibrium modeling data for the removal of RR120 dye onto HSCS, and HSSA at variable initial concentration ranging between 10 and 100 mg/L.

			RR120 dye	
Material	Isotherm	Parameters	Value	R^2
HSCS	Langmuir	q_m (mg/g)	79.35	0.99
		K_L (L/mg)	0.02	
	Freundlich	K_f (mg/g)	4.00	0.96
		n	1.24	
HSSA	Langmuir	q_m (mg/g)	60.27	0.99
		K_L (L/mg)	0.97	
	Freundlich	K_f (mg/g)	4.16	0.95
		n	1.79	

Table 2
Literature pertaining the separation of RR120 dye using various adsorbents.

Adsorbent	pH	q_e (mg/g)	Reference
Ch-Fe	3.6	361.9	(Demarchi et al., 2013)
Chitosan/modified montmorillonite	5	5.610	(Kittinaovarat et al., 2010)
CHS-ECH/ZL	6	284.2	(Jawad et al., 2020b)
Chitosan nanodispersion	5	910	(Momenzadeh et al., 2011)
Chitosan beads	10	129.9	(Mubarak et al., 2017)
Sodium alginate/poly(N-vinyl-2-pyrrolidone)	3	116.8	(İnal and Erduran, 2015)
Fouchana-HDTMA	6	163.9	(Nejib et al., 2015)
Bentonite modified CTAB	3.5	51.2	(Rubai et al., 2021)
Cotton shell	6.5	33.3	(Ashadevi et al., 2011)
Neem bark	6.3	34.3	(Ashadevi et al., 2011)
HSCS	3	79.35	Present Study
HSSA	5	60.27	

$$\text{Langmuir isotherm model}: q_e = \frac{q_m K_L C_e}{1 + K_L C_e} \quad (3)$$

$$\text{Freundlich isotherm model}: q_e = K_f C_e^{1/n} \quad (4)$$

C_e is the equilibrium concentration in milligrams per liter, q_e is the amount absorbed per unit of adsorbent in milligrams per gram, K_L is the volumetric capacity of the adsorbent in liters per gram. The initial concentration of RR120 was adjusted in the range of 10–100 mg/L with pH 3 (HSCS), 5 (HSSA) at 325 °C. Fig. 6 shows the non-linear graphs of the equations corresponding to the analyzed isotherm models (a-b). Table 1 displays the determined values of the constants, isotherm

Table 3
Kinetic modeling of data for the separation of RR120 using HSCS, and HSSA at the dye concentration of 50 ppm and variable temperature ranges between 298 and 318 K.

Adsorbate	T (K)	Pseudo-first order kinetic model				Pseudo-second order kinetic model		
		$q_{e,\ exp}$ (mg/g)	$q_{e1,\ cal}$ (mg/g)	k_1 (1/min)	R^2	$q_{e2,\ cal}$ (mg/g)	k_2 (g/mg min)	R^2
HSCS	298	38.11	33.38	0.04	0.96	39.50	0.02	0.99
	308	40.18	36.51	0.55	0.97	41.22	0.28	0.99
	318	42.94	39.74	0.10	0.97	43.15	0.85	0.99
HSSA	298	26.51	31.32	1.21	0.96	27.83	0.62	0.99
	308	30.68	35.17	0.94	0.95	31.49	0.38	0.99
	318	34.27	39.08	0.92	0.97	35.35	0.30	0.99

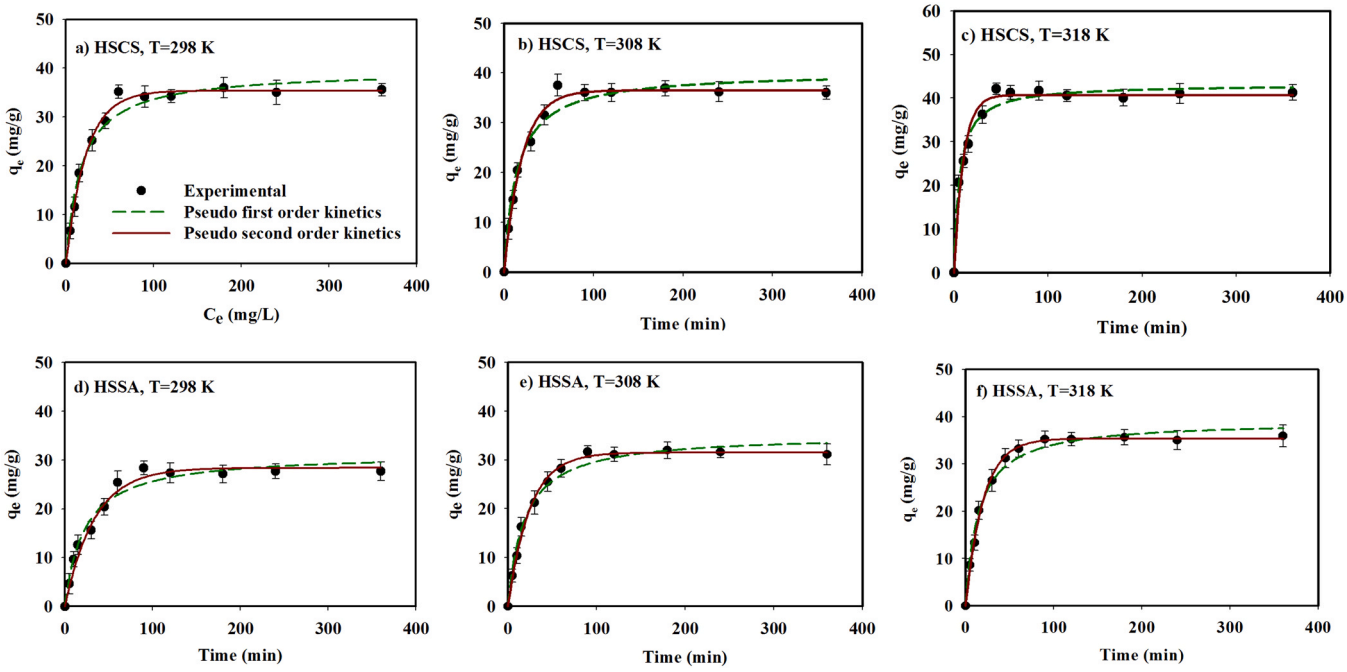

Fig. 7. Nonlinear kinetic studies on separating RR120 dye onto HSCS, HSSA at variable temperatures between 298 and 318 K.

parameters Q_0, and K_l. The Langmuir model is preferable than the Freundlich model for describing the adsorption equilibrium of RR120 dye onto HSCS, and HSSA because it has a higher R^2 value (0.99 vs. 0.94). This suggested that the adsorption occurs as the monolayer (Armbruster and Austin, 1938) dyes adsorbed onto the homogeneous adsorbent surface. In addition, Table 2 provides an overview of the research on RR120 adsorption utilizing different media.

3.10. Effect of contact time

For the purpose of defining the equilibrium contact time, we added 30 mg/L of RR120 solution to each fraction and maintained the chitosan, alginate modified biomass adsorbent quantity at 0.08 g (HSCS) and 0.10 g (HSSA). Because of the higher concentration of the RR120 dye and the availability of the unoccupied sites, the adsorption phenomenon was observed to be rapid during the first phase (0–45 min). Further increasing the residence time to 60 min, the adsorption tends to stabilize or seems to be linear attaining maximum filing up of the vacant sites thereby attaining equilibrium (see Fig. 5(e-f)). Further checking the progress of the adsorption time beyond 60–360 min, there seems to be an equilibrium pattern with no change identified attributed to saturation of active sites. Similarly, the sodium alginate functionalized biomass reported the similar patterns of the increasing during the initial phase i.e., 0–90 min; and attained equilibrium thereafter (90–360 min). This suggests that the 60 min is optimal for HSCS, and 90 min for HSSA and the same has been used throughout the adsorption experiments.

3.11. Kinetic studies

Kinetic studies are required to comprehend the adsorption mechanism and evaluate the performance of HSCS and HSSA adsorbents for RR120 adsorption. Dye RR120 adsorption capacity was shown to increase with time until equilibrium was reached, which occurred within 60 min (HSCS), 90 min (HSCS), and 120 min (HSCS) (HSSA). Within 60 min (HSCS), 99% of the RR120 dye was removed, and no further alterations were seen after that. Two common models for analyzing solid-liquid adsorption are the pseudo-first order (Lagergren, 1989) Eq. (5), and pseudo-second order (Ho and McKay, 1999) Eq. (6) kinetic models.

$$\text{PFO kinetics}: q_t = q_{e1}(1 - \exp(-k_1 t)) \tag{5}$$

$$\text{PSO kinetics}: q_t = \frac{q_{e2}^2 k_2 t}{1 + q_{e2} k_2 t} \tag{6}$$

Where k_1, k_2 (g/mg min) determines the rate constants of kinetic models, and q_t (mg/g) represents the sorption of RR120 onto the unit mass of sorbate surface respectively. Table 3 lists the comparison of experimental and model fit data. From Fig. 7(a-f) and Table 3, higher R^2 value for the pseudo-second order (0.99) kinetic model was reported than that of the pseudo-first order model for both the sorbate (HSSC, and

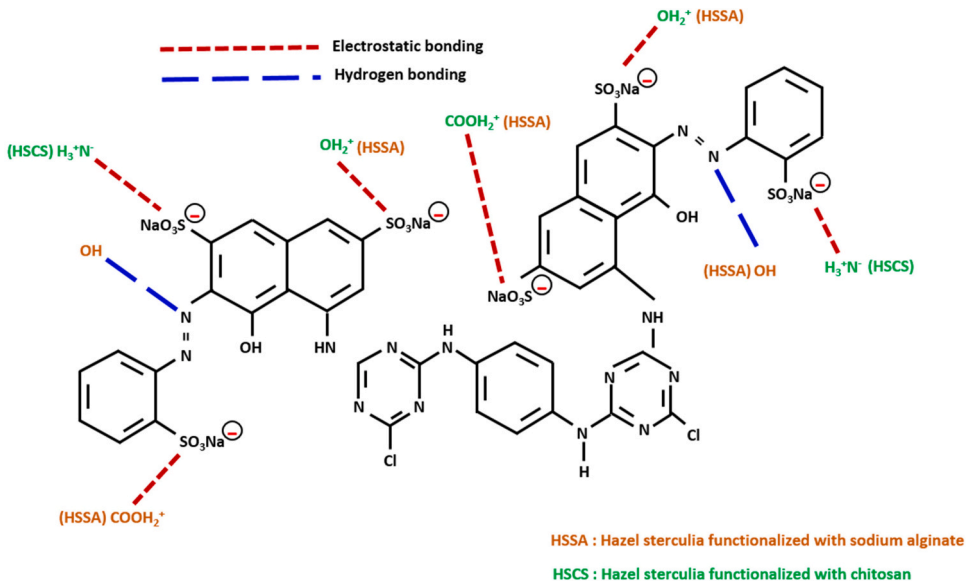

Fig. 8. Adsorption mechanism of RR 120 dye on HSCS, HSSA at optimal adsorption conditions.

HSSA) indicating adsorption of RR120 onto HSCS, HSSA is well described by a pseudo-second order equation demonstrates that chemical adsorption is the rate-limiting step (Vergara-Sánchez et al., 2009).

3.12. Adsorption mechanism

Physical adsorption, precipitation, complexation, and ion-exchange are all methods that can be used to extract dyes from water. Adsorption rates, however, depend on whether or not the poly-bio composites surface features any functional groups or activation sites (Manyatshe et al., 2022). The adsorption mechanism of the RR120 dye on the HSCS, HSSA surface involves both the electrostatic interactions, and hydrogen bonding. Electrostatic repulsion was created between the protonated amino ($–NH_3^+$) and hydroxyl (–OH) groups on the HSCS, HSSA surface and (SO_3^-) functional group of the RR120. Fig. 8 presents a detailed reaction mechanism between the polymer functionalized biomass (HSCS, HSSA) and the dye molecule RR120.

Further, under acidic conditions (pH<7) there are more free protons to protonate the amino groups of chitosan molecules, forming $-NH_3^+$, which strengthens the electrostatic contacts between the negatively charged dye anions and the positively charged adsorption sites (Britto et al., 2021). Moreover, the high density of hydrogen bonds in chitosan is responsible for the broad adsorption band between 3000 and 3600 cm^{-1}, which is created by the superposition of the stretching vibration of the adsorption peaks of $–NH_2$ and –OH (Jiang et al., 2022). After being functionalized onto the surface of the biomass, the intensity of the peak was changed indicating that the hydrogen bonds of the chitosan molecules were altered by the addition of the biomass.

When the pH of sodium alginate is lowered, the hydroxyl and carboxyl groups become ionized, and the carboxyl groups become more protonated, increasing interactions with anionic dyes and strengthening the adsorption phenomena. Hydrogen bonding between sorbate and sorbent molecules is facilitated by the presence of C–H and –OH bonds, thus enhancing the adsorption process (Gollakota et al., 2022). However, the contact forces between sodium alginate molecules are greater due to the strength of the hydrogen bonds between them (Isogai et al., 2011). It is possible that the interaction between alginate and biomass (HSSA) occurs via intermolecular hydrogen bonds, as the peak at 3600–3200 cm^{-1} (O–H stretching vibration) (Sabater i Serra et al., 2020) was slightly shifted to lower wave numbers and widened after alginate was incorporated into biomass. The presence of hydrogen bonds between oxygen-containing groups in alginate chains and biomass, as shown in FTIR spectra, provided more evidence for the close relationship between alginate and biomass. This provided an overview of the

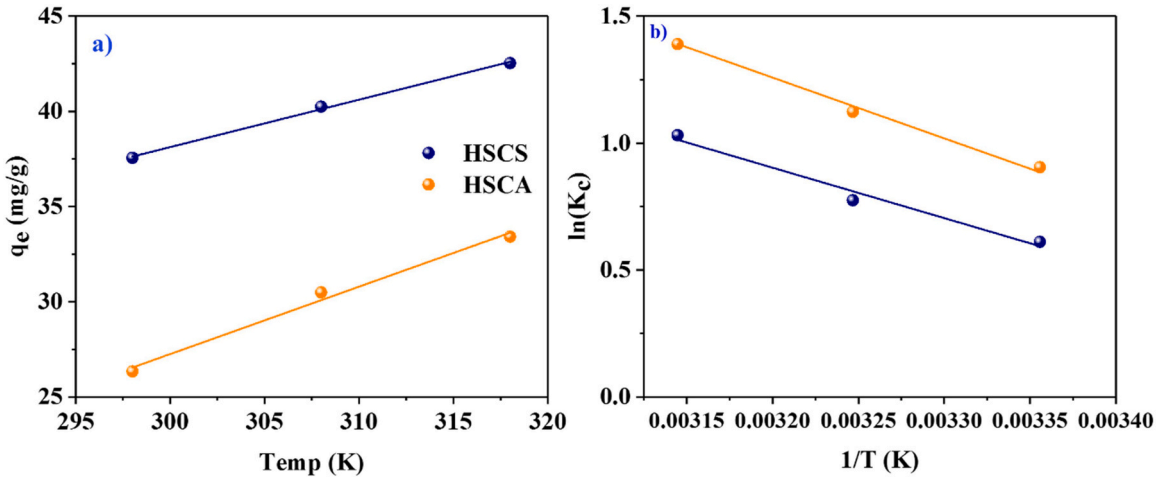

Fig. 9. (a) Thermodynamic studies on the adsorption of RR120 dye onto HSCS, HSCA, (b) Van't Hoff plot for the adsorption of RR120 dye onto HSCS, HSSA.

Table 4
Thermodynamic aspects on adsorption of RR120 dye onto HSCS, and HSSA.

Adsorbate	T (K)	ΔG° (kJ/mol)	ΔH° (kJ/mol)	ΔS° (J/mol K)
HSCS	298	-1.51	19.90	71.88
	308	-1.98		
	318	-2.72		
HSSA	298	-2.29	16.51	63.12
	308	-2.72		
	318	-3.62		

chemistry and mechanism involved in the adsorption in functionalization of chitosan, sodium alginate onto the surface of the biomass towards the separation of RR120 dye involved a complex phenomenon of both electrostatic attraction and the hydrogen bonding of HSCS, HSSA towards the RR120.

3.13. Adsorption thermodynamics

The first principle of thermodynamics states that in a closed system, energy is conserved and entropy always rises as a result of irreversible reactions. To quantify the adsorption process, the reaction temperature must be considered. As a result, the reaction temperature is a major factor in determining how well to predict adsorption phenomena. As a result, many series of experiments were performed on the adsorption process of RR120 dye molecules onto the surface of HSCS, HSSA adsorbents at temperatures ranging from 298 to 318 K while holding all other adsorption factors constant. Fig. 9(a-b) displays an increase in adsorption capacity with increasing temperature, indicating that at higher temperatures, the adsorbent, adsorption sites, and activity were all undergoing chemical changes. Because of this, there was a greater rate of mass transfer from the molecular volume to the limit layer on the molecular surface of the sorbent (Blackburn, 2004). This was due to the fact that the temperature had affected the way in which sorbate molecules diffuse. Elevating the temperature promoted intermolecular interactions between the adsorbed and adsorbed molecules, allowing one to test for improved mobility towards the adsorbing surface. The evaluation of the Gibbs free energy change, enthalpy, and entropy can shed light on the practicability, spontaneity, and heat change of the bio sorption process. Expressions in mathematics for these thermodynamic variables are as follows:

$$\Delta G^0 = -RT\ln K_c \tag{7}$$

$$K_c = \frac{C_{Ae}}{C_e} \tag{8}$$

$$\Delta G^0 = \Delta H^0 - T\Delta S^0 \tag{9}$$

$$\ln K_c = -\frac{\Delta G^0}{RT} = -\frac{\Delta H^0}{RT} + \frac{\Delta S^0}{R} \tag{10}$$

Where R and T represent the universal gas constant (J/molK), T represents the absolute temperature (K), K_c represents the distribution coefficient, and CA_e and C_e represent the equilibrium concentrations (mg/L) of the RR120 dye molecule on the sorbents HSCS and HSSA, respectively. In Fig. 9b, the slope and intercept of a plot of ln Kc vs I/T reveal the thermodynamic parameters (ΔG^0, ΔH^0, ΔS^0) which are detailed in Table 4. The endothermic adsorption process of RR120 is demonstrated by the positive values of ΔH^0, and the increased disorderness of the solid-liquid interface is revealed by the positive value of ΔS^0 (Abdul Hassan et al., 2022). Further, having a negative Gibbs free energy, ΔG^0 indicates that the dye adsorption process was spontaneous and thermodynamically favorable, also supported by the positive value of ΔS^0 i.e., demonstrated by an increase in $\ln K_c$ upon increasing the temperature.

3.14. Desorption and regeneration studies

Adsorbent efficiency is measured, in part, by its ability to be regenerated, which is important from practical, economic, and environmental perspectives. Adsorbents with excellent adsorption and desorption capabilities enhance adsorption process efficacy. Furthermore, desorption rate is proportional to driving force, therefore desorption kinetics were critical for modeling contaminant movement. It is also economically significant to identify a suitable solvent for reusing the adsorbent, as well as to identify environmentally acceptable and/or low-cost adsorbents. Separate dye-saturated HSCS and HSSA solutions were added to the eluent, and the mixture was then shaken for a predetermined period of time to facilitate the desorption process, at which point the dye is removed onto the eluent. The desorbed reactive dye concentration was determined after extraction and adsorbent separation by filtration. For this study, we used NaOH, HNO_3, and HCl, and KOH as acidic, and alkaline eluents respectively, to conduct adsorption and desorption tests (see Fig. 10a). Figure shows that the desorption of HSCS and HSSA from the sorbate (RR120) dye solution is much enhanced in an alkaline medium. NaOH is a more effective eluent for desorbing RR 120 since the dye was anionic. This indicated that desorption of HSCS, HSSA from RR120 dye solution was enhanced by increasing the OH^- ion in the aqueous solution (Choi, 2017) with a greater concentration of NaOH.

The subsequent phase of regeneration is reusability, which is once again tied to economics and provides vital information regarding the adsorption mechanism. Thus, the test for reusability was conducted using HSCS and HSSA in five adsorption/desorption cycles at ideal pH,

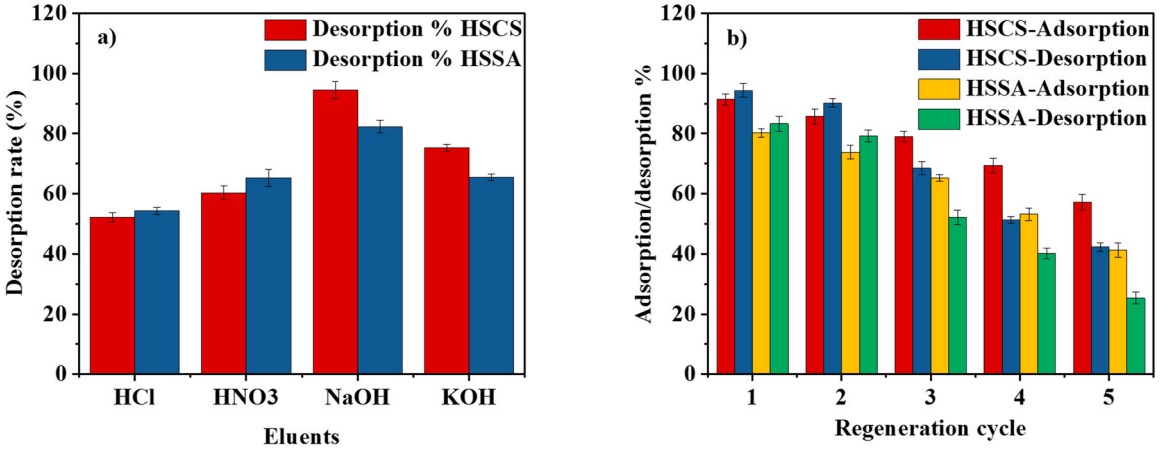

Fig. 10. (a) Desorption of RR120 dye using different eluents (b) regeneration cycles.

temperature, dose, agitation speed, concentration, and time conditions. After each adsorption process, the saturated adsorbents (HSCS, HSSA) were removed from the dye solution and oven-dried at 60 °C for 12 h. Then, it was utilized for the subsequent run under identical conditions (see Fig. 10b). The graph reveals that HSCS adsorbent demonstrates superior performance for the first three cycles, after which the separation efficiency decreased. While HSSA was reported to be effective for two cycles, its efficacy decreased subsequently.

4. Conclusion

Polymer (chitosan (CS), sodium alginate (SA)) functionalized biomass Hazel sterculia seed (HS) adsorbent was prepared to adsorb reactive red 120 dye molecule from effluent streams. Batch sorption studies showed that monolayer adsorption dominated RR120 absorption onto the HSCS, HSSA. Nonlinear analysis of HSCS, HSSA adsorption kinetics, and equilibrium data showed that the pseudo-second order model fits experimental data. Moreover, the thermodynamic studies confirmed the endothermic and spontaneous adsorption reaction mechanism. Besides, alkaline eluent (NaOH) promoted sorbent molecule desorption and reuse during RR120 uptake and the sorbent HSCS can be reused for three cycles, HSSA for two cycles respectively. This suggested that functionalizing polymers onto biomass may be a new way to generate innovative sorbent materials for treating effluent streams with cationic and anionic dyes.

Declaration of Competing Interest

The authors declare that they have no known competing financial interests or personal relationships that could have appeared to influence the work reported in this paper.

Acknowledgement

The authors sincerely appreciate the timely help and cooperation of PS&DPL group.

References

Abdolrahimi, M., Seifi, M., Ramezanzadeh, M.H., 2018. Study the effect of acetic acid on structural, optical and mechanical properties of PVA/chitosan/MWCNT films. Chin. J. Phys. 56, 221–230. https://doi.org/10.1016/j.cjph.2017.12.018.

Abdul Hassan, M.M., Hassan, S.S., Hassan, A.K., 2022. Green and chemical synthesis of bimetallic nanoparticles (Fe/Ni) supported by zeolite 5A as aheterogeneous fenton-like catalyst and study of kinetic and thermodynamic reaction for decolorization of reactive red 120 dye from aqueous pollution. Eurasia Chem. Commun. 4, 1062–1086. https://doi.org/10.22034/ecc.2022.342067.1466.

Abid, S., Uzair, B., Niazi, M.B.K., Fasim, F., Bano, S.A., Jamil, N., Batool, R., Sajjad, S., 2021. Bursting the virulence traits of MDR strain of Candida albicans using sodium alginate-based microspheres containing nystatin-loaded MgO/CuO nanocomposites. Int. J. Nanomed. 16, 1157–1174.

Acquah, G.E., Via, B.K., Fasina, O.O., Eckhardt, L.G., 2016. Rapid quantitative analysis of forest biomass using fourier transform infrared spectroscopy and partial least squares regression. J. Anal. Methods Chem. 2016, 1–10. https://doi.org/10.1155/2016/1839598.

Adel, A.M., El-Shafei, A.M., Ibrahim, A.A., Al-Shemy, M.T., 2019. Chitosan/nanocrystalline cellulose biocomposites based on date palm (Phoenix dactylifera L.) sheath fibers. J. Renew. Mater. 7, 567–582. https://doi.org/10.32604/jrm.2019.00034.

Ahmadi, A., Foroutan, R., Esmaeili, H., Peighambardoust, S.J., Hemmati, S., Ramavandi, B., 2022. Montmorillonite clay/starch/CoFe2O4 nanocomposite as a superior functional material for uptake of cationic dye molecules from water and wastewater. Mater. Chem. Phys. 284, 126088 https://doi.org/10.1016/j.matchemphys.2022.126088.

Al-Tohamy, R., Ali, S.S., Li, F., Okasha, K.M., Mahmoud, Y.A.G., Elsamahy, T., Jiao, H., Fu, Y., Sun, J., 2022. A critical review on the treatment of dye-containing wastewater: Ecotoxicological and health concerns of textile dyes and possible remediation approaches for environmental safety. Ecotoxicol. Environ. Saf. 231, 113160 https://doi.org/10.1016/j.ecoenv.2021.113160.

Anfar, Z., Ait Ahsaine, H., Zbair, M., Amedlous, A., Ait El Fakir, A., Jada, A., ElAlem, N., 2020. Recent trends on numerical investigations of response surface methodology for pollutants adsorption onto activated carbon materials: a review. Crit. Rev. Environ. Sci. Technol. 50, 1043–1084. https://doi.org/10.1080/10643389.2019.1642835.

Armbruster, M.H., Austin, J.B., 1938. The adsorption of gases on plane surfaces of mica. J. Am. Chem. Soc. 60, 467–475. https://doi.org/10.1021/ja01269a066.

Ashadevi, U., Immanuel, V.P., Usharani, T., 2011. Fixed bed column study for the removal of reactive red 120(RR120) dye from aquatic environment by low cost adsorbents. Proc. Int. Conf. Green Technol. Environ. Conserv. GTEC-2011 120, 347–355. https://doi.org/10.1109/GTEC.2011.6167692.

Awoyale, A.A., Lokhat, D., 2021. Experimental determination of the effects of pretreatment on selected Nigerian lignocellulosic biomass in bioethanol production. Scientific Reports 11, 1–16. https://doi.org/10.1038/s41598-020-78105-8.

Bat-Amgalan, M., Khashbaatar, Z., Anak, D.E.V., Sari, M.N.M., Miyamoto, N., Kano, N., Kim, H.-J., Yunden, G., 2021. Adsorption of Cr(III) from an Aqueous Solution by Chitosan Beads Modified with Sodium Dodecyl Sulfate (SDS). J. Environ. Prot. (Irvine,. Calif.) 12, 939–960. https://doi.org/10.4236/jep.2021.1211055.

Bazrafshan, E., Ahmadabadi, M., Mahvi, A.H., 2013. Reactive red-120 removal by activated carbon obtained from cumin herb wastes. Fresenius Environ. Bull. 22, 584–590.

Bekiaris, G., Tagkouli, D., Koutrotsios, G., Kalogeropoulos, N., Zervakis, G.I., 2020. Pleurotus mushrooms content in glucans and ergosterol assessed by ATR-FTIR spectroscopy and multivariate analysis. Foods 9. https://doi.org/10.3390/foods9040535.

Bensalah, H., Bekheet, M.F., Younssi, S.A., Ouammou, M., Gurlo, A., 2017. Removal of cationic and anionic textile dyes with Moroccan natural phosphate. J. Environ. Chem. Eng. 5, 2189–2199. https://doi.org/10.1016/j.jece.2017.04.021.

Blackburn, R.S., 2004. Natural polysaccharides and their interactions with dye molecules: applications in effluent treatment. Environ. Sci. Technol. 38, 4905–4909. https://doi.org/10.1021/es049972n.

Britto, J., Barani, P., Vanaja, M., Pushpalaksmi, E., Jenson Samraj, J., Annadurai, G., 2021. Adsorption of dyes by chitosan-selenium nanoparticles: recent developments and adsorption mechanisms. Nat. Environ. Pollut. Technol. 20, 467–479. https://doi.org/10.46488/NEPT.2021.v20i02.003.

Choi, H.J., 2017. Application of surface modified sericite to remove anionic dye from an aqueous solution. Environ. Eng. Res 22, 312–319. https://doi.org/10.4491/eer.2016.156.

Demarchi, C.A., Campos, M., Rodrigues, C.A., 2013. Adsorption of textile dye Reactive Red 120 by the chitosan-Fe(III)- crosslinked: Batch and fixed-bed studies. J. Environ. Chem. Eng. 1, 1350–1358. https://doi.org/10.1016/j.jece.2013.10.005.

El-Hefian, E.A., Nasef, M.M., Yahaya, A.H., 2010. The preparation and characterization of Chitosan / Poly (Vinyl Alcohol) blended films. E-J. Chem. 7, 1212–1219. https://doi.org/10.1155/2010/626235.

Foroutan, R., Peighambardoust, S.J., Aghdasinia, H., Mohammadi, R., Ramavandi, B., 2020. Modification of bio-hydroxyapatite generated from waste poultry bone with MgO for purifying methyl violet-laden liquids. Environ. Sci. Pollut. Res. 27, 44218–44229. https://doi.org/10.1007/s11356-020-10330-0.

Foroutan, R., Peighambardoust, S.J., Esvandi, Z., Khatooni, H., Ramavandi, B., 2021. Evaluation of two cationic dyes removal from aqueous environments using CNT/MgO/CuFe2O4magnetic composite powder: A comparative study. J. Environ. Chem. Eng. 9, 104752 https://doi.org/10.1016/j.jece.2020.104752.

Freundlich, V.H., 1907. Kolloidfiillung und Adsorption. Juretzka Gattierung von Zinkblende und Galmei. 20, 750–754. https://doi.org/10.1002/ange.19070201806.

Gaabour, L.H., 2017. Spectroscopic and thermal analysis of polyacrylamide/chitosan (PAM/CS) blend loaded by gold nanoparticles. Results Phys. 7, 2153–2158. https://doi.org/10.1016/j.rinp.2017.06.027.

Gao, X., Guo, C., Hao, J., Zhao, Z., Long, H., Li, M., 2020. Adsorption of heavy metal ions by sodium alginate based adsorbent-a review and new perspectives. Int. J. Biol. Macromol. 164, 4423–4434. https://doi.org/10.1016/j.ijbiomac.2020.09.046.

Geethakarthi, A., Phanikumar, B.R., 2011. Adsorption of reactive dyes from aqueous solutions by tannery sludge developed activated carbon: Kinetic and equillibrium studies. Int. J. Environ. Sci. Tech. 8, 561–570.

Gollakota, A., Munagapati, V., Liao, S., Shu, C., Shadangi, K., Sarangi, P., Wen, J., 2023. Ionic liquid [bmim] [TFSI] templated Na-X zeolite for the adsorption of (Cd^{2+}, Zn^{2+}), and dyes (AR, R6). Environ. Res 216, 114525.

Gollakota, A.R.K., Subbaiah, V., Volli, V., Gautam, S., Wen, J., Shu, C., 2021. Coal bottom ash derived zeolite (SSZ-13) for the sorption of synthetic anion Alizarin Red S (ARS) dye. J. Hazard. Mater. 416, 125925 https://doi.org/10.1016/j.jhazmat.2021.125925.

Gollakota, A.R.K., Subbaiah Munagapati, V., Shu, C.M., Wen, J.C., 2022. Adsorption of Cr (VI), and Pb (II) from aqueous solution by 1-Butyl-3-methylimidazolium bis (trifluoromethylsulfonyl)imide functionalized biomass Hazel Sterculia (Sterculia foetida L.). J. Mol. Liq. 350, 118534 https://doi.org/10.1016/j.molliq.2022.118534.

Heba, K., Ali, H., 2023. Simultaneous removal of cationic crystal violet and anionic reactive yellow using eco- friendly chitosan functionalized by Talc and Cloisite 30B. J. Polym. Env 31, 1456–1477.

Ho, Y.S., McKay, G., 1999. Pseudo-second order model for sorption processes. Process Biochem 34, 451–465. https://doi.org/10.1021/acs.oprd.7b00090.

Huang, Y.C., Chu, H.W., 2013. Using hydroxyapatite from fish scales to prepare chitosan/gelatin/ hydroxyapatite membrane: exploring potential for bone tissue engineering. J. Mar. Sci. Technol. 21, 716–722. https://doi.org/10.6119/JMST-013-0320-1.

İnal, M., Erduran, N., 2015. Removal of various anionic dyes using sodium alginate/poly (N-vinyl-2-pyrrolidone) blend hydrogel beads. Polym. Bull. 72, 1735–1752. https://doi.org/10.1007/s00289-015-1367-7.

Isogai, A., Saito, T., Fukuzumi, H., 2011. Tempo-oxidized cellulose nanofibers. Nanoscale 3, 71–85. https://doi.org/10.1039/c0nr00583e.

Jawad, A.H., Abdulhameed, A.S., 2020a. Mesoporous Iraqi red kaolin clay as an efficient adsorbent for methylene blue dye: adsorption kinetic, isotherm and mechanism study. Surf. Interfaces 18, 100422. https://doi.org/10.1016/j.surfin.2019.100422.

Jawad, A.H., Abdulhameed, A.S., 2020b. Facile synthesis of crosslinked chitosan-tripolyphosphate/kaolin clay composite for decolourization and COD reduction of remazol brilliant blue R dye: optimization by using response surface methodology. Colloids Surf. A Physicochem. Eng. Asp. 605, 125329 https://doi.org/10.1016/j.colsurfa.2020.125329.

Jawad, A.H., Abdulhameed, A.S., Mastuli, M.S., 2020a. Mesoporous crosslinked chitosan-activated charcoal composite for the removal of thionine cationic dye: comprehensive adsorption and mechanism study. J. Polym. Environ. 28, 1095–1105. https://doi.org/10.1007/s10924-020-01671-5.

Jawad, A.H., Abdulhameed, A.S., Reghioua, A., Yaseen, Z.M., 2020b. Zwitterion composite chitosan-epichlorohydrin/zeolite for adsorption of methylene blue and reactive red 120 dyes. Int. J. Biol. Macromol. 163, 756–765. https://doi.org/10.1016/j.ijbiomac.2020.07.014.

Jawad, A.H., Mubarak, N.S.A., Abdulhameed, A.S., 2020c. Tunable Schiff's base-cross-linked chitosan composite for the removal of reactive red 120 dye: adsorption and mechanism study. Int. J. Biol. Macromol. 142, 732–741. https://doi.org/10.1016/j.ijbiomac.2019.10.014.

Jiang, S., Qiao, C., Wang, X., Li, Z., Yang, G., 2022. Structure and properties of chitosan/sodium dodecyl sulfate composite films. RSC Adv. 12, 3969–3978. https://doi.org/10.1039/d1ra08218c.

Kahya, N., Erim, F.B., 2019. Surfactant modified alginate composite gels for controlled release of protien drug. Carbohydr. Polym. 224 (2019), 115165.

Kaya, M., Seyyar, O., Baran, T., Turkes, T., 2014. Bat guano as new and attractive chitin and chitosan source. Front. Zool. 11, 59. https://doi.org/10.1186/preaccept-2130575587130627.

Kim, S., 2021. Blending of waste biomass for cost-effective chitosan-based biosorbents for removal of reactive dye from aqueous solution, 210457–0 Environ. Eng. Res 27. https://doi.org/10.4491/eer.2021.457.

Kittinaovarat, S., Kansomwan, P., Jiratumnukul, N., 2010. Chitosan/modified montmorillonite beads and adsorption Reactive Red 120. Appl. Clay Sci. 48, 87–91. https://doi.org/10.1016/j.clay.2009.12.017.

Kuczajowska-Zadrożna, M., Filipkowska, U., Jóźwiak, T., 2020a. Adsorption of Cu (II) and Cd (II) from aqueous solutions by chitosan immobilized in alginate beads. J. Environ. Chem. Eng. 8, 103878 https://doi.org/10.1016/j.jece.2020.103878.

Lagergren, S., 1989. Zur theorie der sogenanntan adsorption gloster stoffe. K. Sven. Vetensk. Handl. 24, 1–39.

Langmuir, I., 1918. The adsorption of gases on plane surfaces of glass, mica and platinum. Eucken, Verh. deut. Phys. Ges. 16, 1361–1403. https://doi.org/10.1021/ja01269a066.

Li, H., Jin, R., Hu, H., Kianpoor Kalkhajeh, Y., Zhao, Y., Gao, Y., Zhang, B., 2021. Adsorption of as(iii), pb(ii), and zn(ii) from wastewater by sodium alginate modified materials. J. Anal. Methods Chem. 2021. https://doi.org/10.1155/2021/7527848.

Liu, Y., He, Z., Shankle, M., Tewolde, H., 2016. Compositional features of cotton plant biomass fractions characterized by attenuated total reflection Fourier transform infrared spectroscopy. Ind. Crops Prod. 79, 283–286. https://doi.org/10.1016/j.indcrop.2015.11.022.

Lowell, S., Shields, J.E., 1991. Adsorption isotherms. Powder Surf. Area Porosity 11–13. https://doi.org/10.1007/978-94-015-7955-1_3.

Mansfield, J., Eislet, P., Yeh, J., Mooney, D.J., 1999. Environmental SEM study of Sodium Alginate beads. microscopy. Micoanalys 5 (S2), 300–301.

Manyatshe, A., Cele, Z.E.D., Balogun, M.O., Nkambule, T.T.I., Msagati, T.A.M., 2022. Lignocellulosic derivative-chitosan biocomposite adsorbents for the removal of soluble contaminants in aqueous solutions – preparation, characterization and applications. J. Water Process Eng. 47, 102654 https://doi.org/10.1016/j.jwpe.2022.102654.

Mishra, D., Nagpal, M., Singh, S., 2013. Superporous hybrid hydrogels based on polyacrylamide and chitosan: characterization and in vitro drug release. Int. J. Pharm. Invest. 3, 88. https://doi.org/10.4103/2230-973x.114906.

Mohammed, C., Lalgee, L., Kistow, M., Jalsa, N., Ward, K., 2022. On the binding affinity and thermodynamics of sodium alginate-heavy metal ion interactions for efficient adsorption. Carbohydr. Polym. Technol. Appl. 3, 100203 https://doi.org/10.1016/j.carpta.2022.100203.

Momenzadeh, H., Tehrani-Bagha, A.R., Khosravi, A., Gharanjig, K., Holmberg, K., 2011. Reactive dye removal from wastewater using a chitosan nanodispersion. Desalination 271, 225–230. https://doi.org/10.1016/j.desal.2010.12.036.

Mousavi, S.M., Meraji, S.H., Sanati, A.M., Ramavandi, B., 2023. Phenol red dye removal from wastewater using TiO2-FSM-16 and Ni-FSM-16 photocatalysts. Heliyon 9, e14488. https://doi.org/10.1016/j.heliyon.2023.e14488.

Mubarak, N.S.A., Jawad, A.H., Nawawi, W.I., 2017. Equilibrium, kinetic and thermodynamic studies of Reactive Red 120 dye adsorption by chitosan beads from aqueous solution. Energy, Ecol. Environ. 2, 85–93. https://doi.org/10.1007/s40974-016-0027-6.

Nejib, A., Joelle, D., Fadhila, A., Sophie, G., Malika, T.A., 2015. Adsorption of anionic dye on natural and organophilic clays: effect of textile dyeing additives. Desalin. Water Treat. 54, 1754–1769. https://doi.org/10.1080/19443994.2014.895781.

Nitsos, C., Matsakas, L., Triantafyllidis, K., Rova, U., Christakopoulos, P., 2018. Investigation of different pretreatment methods of Mediterranean-type ecosystem agricultural residues: characterisation of pretreatment products, high-solids enzymatic hydrolysis and bioethanol production. Biofuels 9, 545–558. https://doi.org/10.1080/17597269.2017.1378988.

Pashaei-Fakhri, S., Peighambardoust, S.J., Foroutan, R., Arsalani, N., Ramavandi, B., 2021. Crystal violet dye sorption over acrylamide/graphene oxide bonded sodium alginate nanocomposite hydrogel. Chemosphere 270, 129419. https://doi.org/10.1016/j.chemosphere.2020.129419.

Patra, T., Mohanty, A., Singh, L., Muduli, S., Parhi, P., Sahoo, T., 2022. Effect of calcination temperature on morphology and phase transformation of MnO2 nanoparticles: a step towards green synthesis for reactive dye adsorption. Chemosphere 288, 132472.

Pereira, R., Tojeira, A., Vaz, D.C., Mendes, A., Bártolo, P., 2011. Preparation and characterization of films based on alginate and Aloe vera. Int. J. Polym. Anal. Charact. 16, 449–464. https://doi.org/10.1080/1023666X.2011.599923.

Pourjavadi, A., Nazari, M., Hosseini, S.H., 2015. Synthesis of magnetic graphene oxide-containing nanocomposite hydrogels for adsorption of crystal violet from aqueous solution. RSC Adv. 5, 32263–32271. https://doi.org/10.1039/c4ra17103a.

Rorrer, G.L., Tzu-Yang, H., Way, D.J., 1993. Synthesis of porous-magnetic chitosan beads for removal of cadmium ions from waste water. Ind. Eng. Chem. Res. 32, 2170–2178.

Rubai, H.F., Al, Hassan, A.K., Sultan, M.S., Abood, W.M., 2021. Kinetics of adsorption of reactive red 120 using bentonite modified by CTAB and study the effect of salts. Nat. Environ. Pollut. Technol. 20, 281–289. https://doi.org/10.46488/NEPT.2021.V20I01.031.

Sabater i Serra, R., Molina-Mateo, J., Torregrosa-Cabanilles, C., Andrio-Balado, A., Dueñas, J.M.M., Serrano-Aroca, Á., 2020. Bio-Nanocomposite hydrogel based on zinc alginate/graphene oxide: morphology, structural conformation, thermal behavior/degradation, and dielectric properties. Polym. (Basel) 12 (3), 702. https://doi.org/10.3390/polym12030702.

Sargin, I., Arslan, G., Kaya, M., 2016. Efficiency of chitosan-algal biomass composite microbeads at heavy metal removal. React. Funct. Polym. 98, 38–47. https://doi.org/10.1016/j.reactfunctpolym.2015.11.007.

Sarwar, M.S., Ghaffar, A., Huang, Q., 2021. Development and characterization of sodium alginate/poly(sodium 4-styrenesulfonate) composite films for release behavior of ciprofloxacin hydrogen chloride monohydrate. Polym. Polym. Compos 29, S143–S153. https://doi.org/10.1177/0967391121990278.

Singh, H., Choden, S., 2014. Comparison of adsorption behaviour and kinetic modeling of bio-waste materials using basic dye as adsorbate. Indian J. Chem. Technol. 21, 359–367. https://doi.org/10.1061/9780784412725.ch08.

Sutirman, Z., Sanagi, M., Karim, K., Ibrahim, W., Naim, A., 2018. Chitosan-based adsorbents for the removal of metal ions from aqueous solutions. Malays. J. Anal. Sci. 22, 839–850.

Szygula, A., Ruiz, M., Guibal, E., Sastre, A.M., 2008. Removal of an anionic reactive dye by chitosan and its regeneration. Energy Environ. Eng. Ser. 24–30.

Varma, R., Vasudevan, S., Chelladurai, S., Narayanasamy, A., 2021. Synthesis and physicochemical characteristics of chitosan extracted from Pinna deltoides. Lett. Appl. NanoBioScience 11, 4061–4070. https://doi.org/10.33263/lianbs114.40614070.

Vergara-Sánchez, J., Pérez-Orozco, J.P., Suárez-Parra, R., Hernández-Pérez, I., 2009. Degradation of reactive red 120 azo dye in aqueous solutions using homogeneous/heterogeneous iron systems degradac on del colorante azo rojo reactivo 120 en soluciones acuosas usando sistemas homo eneos/hetero eneos de hierro. Abril Rev. Mex. Ing. Quím. 8, 121–131.

Zhu, L., Guan, C., Zhou, B., Zhang, Z., Yang, R., Tang, Y., Yang, J., 2017. Adsorption of dyes onto sodium alginate graft polyacrylic acid-co-2-acrylamide-2-methyl propane sulfonic acid)/ kaolin hydrogel composite. Polym. Polym. Compos 25, 627–634. https://doi.org/10.1177/096739111702500808.